

---

# Discovering Neural Wirings

---

Mitchell Wortsman<sup>1</sup>, Ali Farhadi<sup>1,2,3</sup>, Mohammad Rastegari<sup>1,3</sup>

<sup>1</sup>PRIOR @ Allen Institute for AI, <sup>2</sup>University of Washington, <sup>3</sup>XNOR.AI  
mitchellw@allenai.org, {ali, mohammad}@xnor.ai

## Abstract

The success of neural networks has driven a shift in focus from feature engineering to architecture engineering. However, successful networks today are constructed using a small and manually defined set of building blocks. Even in methods of neural architecture search (NAS) the network connectivity patterns are largely constrained. In this work we propose a method for discovering neural wirings. We relax the typical notion of layers and instead enable channels to form connections independent of each other. This allows for a much larger space of possible networks. The wiring of our network is not fixed during training – as we learn the network parameters we also learn the structure itself. Our experiments demonstrate that our learned connectivity outperforms hand engineered and randomly wired networks. By learning the connectivity of MobileNetV1 [10] we boost the ImageNet accuracy by 10% at  $\sim 41\text{M}$  FLOPs. Moreover, we show that our method generalizes to recurrent and continuous time networks. Code and pretrained models are available at <https://github.com/allenai/dnw>.

## 1 Introduction

Deep neural networks have shifted the prevailing paradigm from *feature engineering* to *feature learning*. The architecture of deep neural networks, however, must still be hand designed in a process known as *architecture engineering*. A myriad of recent efforts attempt to automate the process of the architecture design by searching among a set of smaller well-known building blocks [24, 27, 30, 16, 1, 17]. While methods of search range from reinforcement learning to gradient based approaches [27, 17], the space of possible connectivity patterns is still largely constrained. NAS methods explore wirings between large blocks. We believe that more efficient solutions may arrive from searching the space of wirings at a more fine grained level, i.e. single channels.

In this work, we consider an unconstrained set of possible wirings by allowing channels to form connections independent of each other. This enables us to discover a wide variety of operations (e.g. depthwise separable convs [10], channel shuffle and split [29], and more). Formally, we treat the network as a large *neural graph* where each node processes a single channel.

One key challenge lies in searching the space of all possible wirings – the number of possible sub-graphs is combinatorial in nature. When considering thousands of nodes, traditional search methods are either prohibitive or offer approximate solutions. In this paper we introduce a simple and efficient algorithm for discovering neural wirings (DNW). Our method searches the space of all possible wirings with a simple modification of the backwards pass.

Most similar to our approach is work in randomly wired neural networks [28] aiming to explore the space of novel neural network wirings. Intriguingly, they show that constructing neural networks with random graph algorithms often outperforms a manually engineered architecture. However, these wirings are fixed at training.

Our method for discovering neural wirings is as follows: First, we consider the sole constraint that that the total number of edges in the *neural graph* is fixed to be  $k$ . Initially we randomly assign a

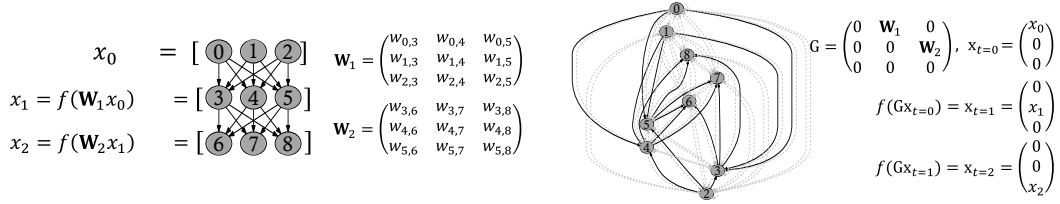


Figure 1: **Dynamic Neural Graph:** A 3-layer perceptron (*left*) can be expressed by a dynamic neural graph with 3 time steps (*right*).

weight to each edge. We then choose the weighted edges with the highest magnitude and refer to the remaining edges as *hallucinated*. As we train, we modify the weights of *all* edges according to a specified update rule. Accordingly, a hallucinated edge may strengthen to a point it replaces a real edge. We tailor the update rule so that when *swapping* does occur, it is beneficial.

We consider the application of DNW for *static* and *dynamic* neural graphs. In the *static* regime each node has a single output and the graphical structure is acyclic. In the case of a *dynamic neural graph* we allow the state of a node to vary with time. *Dynamic neural graphs* may contain cycles and express popular sequential models such as LSTMs [9]. As *dynamic neural graphs* are strictly more expressive than *static neural graphs*, they can also express feed-forward networks (as in Figure 1).

Our work may also be regarded as an effective mechanism for training a sparse network. The *Lottery Ticket Hypothesis* [6, 7] has demonstrated the existence of sparse sub-networks which may be trained in isolation. However, their method for identifying so-called *winning-tickets* is quite expensive and requires multiple passes of training. Though we do not train our networks in isolation (we consider a set of *hallucinated edges*), DNW may be used to train a sparse network in a single pass.

We demonstrate the efficacy of DNW on small and large scale data-sets, and for feed-forward, recurrent, and continuous networks. Notably, we augment MobileNetV1 [10] with DNW to achieve a 10% improvement on ImageNet [4] from the hand engineered MobileNetV1 at  $\sim 41\text{M FLOPs}$ <sup>1</sup>.

## 2 Discovering Neural Wirings

In this section we describe our method for jointly discovering the structure and learning the parameters of a neural network. We first consider the algorithm in a familiar setting, a feed-forward neural network, which we abstract as a *static neural graph*. We then present a more expressive *dynamic neural graph* which extends to discrete and continuous time and generalizes feed-forward, recurrent, and continuous time neural networks.

### 2.1 Static Neural Graph

A *static neural graph* is a directed acyclic graph  $\mathcal{G} = (\mathcal{V}, \mathcal{E})$  consisting of nodes  $\mathcal{V}$  and edges  $\mathcal{E} \subseteq \mathcal{V} \times \mathcal{V}$ . The state of a node  $v \in \mathcal{V}$  is given by the random variable  $Z_v$ . At each node  $v$  we apply a function  $f_{\theta_v}$  and with each edge  $(u, v)$  we associate a weight  $w_{uv}$ . In the case of a multi-layer perceptron,  $f$  is simply a parameter-free non-linear activation like ReLU [14].

For any set  $\mathcal{A} \subseteq \mathcal{V}$  we let  $\mathbf{Z}_{\mathcal{A}}$  denote  $(Z_v)_{v \in \mathcal{A}}$  and so  $\mathbf{Z}_{\mathcal{V}}$  is a vector containing the state of all nodes in the network.

$\mathcal{V}$  contains a subset of input nodes  $\mathcal{V}_0$  with no parents and output nodes  $\mathcal{V}_E$  with no children. The input data  $\mathcal{X} \sim p_x$  flows into the network through  $\mathcal{V}_0$  as  $\mathbf{Z}_{\mathcal{V}_0} = g_{\phi}(\mathcal{X})$  for a function  $g$  which may have parameters  $\phi$ . Similarly, the output of the network  $\hat{\mathcal{Y}}$  is given by  $h_{\psi}(\mathbf{Z}_{\mathcal{V}_E})$ .

$$Z_v = \begin{cases} f_{\theta_v} \left( \sum_{(u,v) \in \mathcal{E}} w_{uv} Z_u \right) & v \in \mathcal{V} \setminus \mathcal{V}_0 \\ g_{\phi}^{(v)}(\mathcal{X}) & v \in \mathcal{V}_0. \end{cases} \quad (1)$$

<sup>1</sup>We follow [29, 19] and define FLOPS as the number of Multiply Adds.

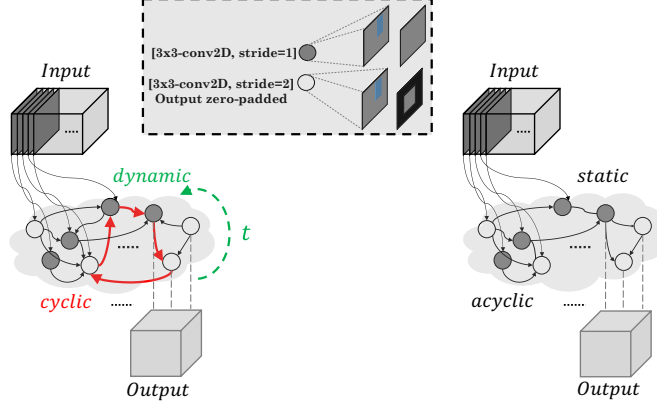


Figure 2: An example of a dynamic (left) and static (right) neural graph. Details in Section 2.3.

For brevity, we let  $\mathcal{I}_v$  denote the “input” to node  $v$ , where  $\mathcal{I}_v$  may be expressed

$$\mathcal{I}_v = \sum_{(u,v) \in \mathcal{E}} w_{uv} Z_u. \quad (2)$$

In this work we consider the case where the input and output of each node is a two-dimensional matrix, commonly referred to as a channel. Each node performs a non-linear activation followed by normalization and convolution (which may be strided to reduce the spatial resolution). As in [28], we no longer conform to the traditional notion of “layers” in a deep network.

The combination of a separate  $3 \times 3$  convolution for each channel (depthwise convolution) followed by a  $1 \times 1$  convolution (pointwise convolution) is often referred to as a depthwise separable convolution, and is essential in efficient network design [10, 19]. With a *static neural graph* this process may be interpreted equivalently as a  $3 \times 3$  convolution at each node followed by information flow on a complete bipartite graph.

## 2.2 Discovering a $k$ -Edge neural graph

We now outline our method for discovering the edges of a static neural graph subject to the constraint that the total number of edges must not exceed  $k$ .

We consider a set of real edges  $\mathcal{E}$  and a set of *hallucinated* edges  $\mathcal{E}_{\text{hal}} = \mathcal{V} \times \mathcal{V} \setminus \mathcal{E}$ . The real edge set is comprised of the  $k$ -edges which have the largest magnitude weight. As we allow the magnitude of the weights in both sets to change throughout training the edges in  $\mathcal{E}_{\text{hal}}$  may replace those in  $\mathcal{E}$ .

Consider a *hallucinated* edge  $(u, v) \notin \mathcal{E}$ . If the gradient is pushing  $\mathcal{I}_v$  in a direction which aligns with  $Z_u$ , then our update rule strengthens the magnitude of the weight  $w_{uv}$ . If this alignment happens consistently then  $w_{uv}$  will be eventually be strong enough to enter the real edge set  $\mathcal{E}$ . As the total number of edges is conserved, when  $(u, v)$  enters the edge set  $\mathcal{E}$  another edge is removed and placed in  $\mathcal{E}_{\text{hal}}$ . This procedure is detailed by Algorithm 1, where  $\mathcal{V}$  is the node set,  $\mathcal{V}_0, \mathcal{V}_E$  are the input and output node sets,  $g_\phi, h_\psi$  and  $\{f_{\theta_v}\}_{v \in \mathcal{V}}$  are the input, output, and node functions,  $p_{xy}$  is the data distribution,  $k$  is the number of edges in the graph and  $\mathcal{L}$  is the loss.

In practice we may also include a momentum and weight decay<sup>2</sup> term in the weight update rule (line 10 in Algorithm 1). In fact, the weight update rule looks nearly identical to that in traditional SGD & Backprop but for one key difference: we **allow** the gradient to flow *to* edges which did not exist during the forwards pass. Importantly, we **do not allow** the gradient to flow *through* these edges and so the rest of the parameters update as in traditional SGD & Backprop. This gradient flow is illustrated in Figure 3.

Under certain conditions we formally show that swapping an edge from  $\mathcal{E}_{\text{hal}}$  to  $\mathcal{E}$  decreases the loss  $\mathcal{L}$ . We first consider the simple case where the *hallucinated edge*  $(i, k)$  replaces  $(j, k) \in \mathcal{E}$ . In Section C we discuss the proof to a more general case.

<sup>2</sup>Weight decay [15] may in fact be very helpful for eliminating dead ends.

---

**Algorithm 1** DNW-Train( $\mathcal{V}, \mathcal{V}_0, \mathcal{V}_E, g_\phi, h_\psi, \{f_{\theta_v}\}_{v \in \mathcal{V}}, p_{xy}, k, \mathcal{L}$ )

---

- 1: **for** each pair of nodes  $(u, v)$  such that  $u < v$  **do** ▷ Initialize
  - 2:     Initialize  $w_{uv}$  by independently sampling from a uniform distribution.
  - 3: **for** each training iteration **do**
  - 4:     Sample mini batch of data and labels  $(\mathcal{X}, \mathcal{Y}) = \{(\mathcal{X}_i, \mathcal{Y}_i)\}$  using  $p_{xy}$  ▷ Sample data
  - 5:      $\mathcal{E} \leftarrow \{(u, v) \in \mathcal{V} \times \mathcal{V} : |w_{uv}| \geq \tau\}$  where  $\tau$  is chosen so that  $|\mathcal{E}| = k$  ▷ Choose edges
  - 6:      $Z_v \leftarrow \begin{cases} f_{\theta_v} \left( \sum_{(u,v) \in \mathcal{E}} w_{uv} Z_u \right) & v \in \mathcal{V} \setminus \mathcal{V}_0 \\ g_\psi^{(v)}(\mathcal{X}) & v \in \mathcal{V}_0 \end{cases}$  ▷ Forward pass
  - 7:      $\hat{\mathcal{Y}} = h_\psi(\{Z_v\}_{v \in \mathcal{V}_E})$  ▷ Compute output
  - 8:     Update  $\phi, \{\theta_v\}_{v \in \mathcal{V}}, \psi$  via SGD & Backprop [21] using loss  $\mathcal{L}(\hat{\mathcal{Y}}, \mathcal{Y})$
  - 9:     **for** each pair of nodes  $(u, v)$  such that  $u < v$  **do** ▷ Update edge weights
  - 10:          $w_{uv} \leftarrow w_{uv} + \left\langle Z_u, -\alpha \frac{\partial \mathcal{L}}{\partial \mathcal{I}_v} \right\rangle$  ▷ Recall  $\mathcal{I}_v = \sum_{(u,v) \in \mathcal{E}} w_{uv} Z_u$
- 

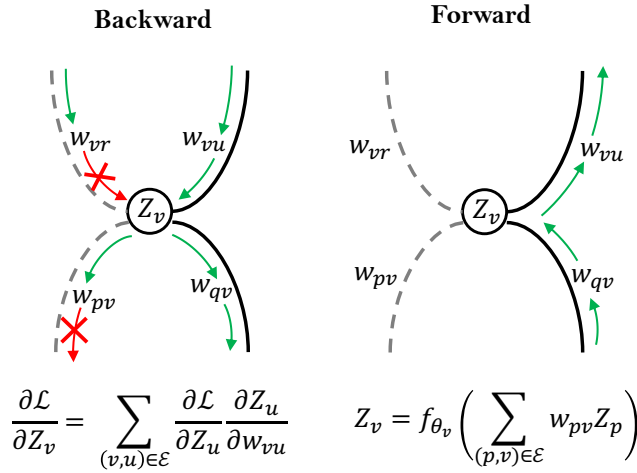


Figure 3: **Gradient flow:** On the forwards pass we use only on the *real* edges. On the backwards pass we allow the gradient to flow *to* but not *through* the hallucinated edges (as in Algorithm 1).

We let  $\tilde{w}$  to denote the weight  $w$  after the weight update rule  $\tilde{w}_{uv} = w_{uv} + \left\langle Z_u, -\alpha \frac{\partial \mathcal{L}}{\partial \mathcal{I}_v} \right\rangle$ . We assume that  $\alpha$  is small enough so that  $\text{sign}(\tilde{w}) = \text{sign}(w)$ .

**Claim:** Assume  $\mathcal{L}$  is Lipschitz continuous. There exists a learning rate  $\alpha^* > 0$  such that for  $\alpha \in (0, \alpha^*)$  the process of swapping  $(i, k)$  for  $(j, k)$  will decrease the loss when the state of the nodes are fixed and  $|w_{ik}| < |w_{jk}|$  but  $|\tilde{w}_{ik}| > |\tilde{w}_{jk}|$ .

*Proof.* Let  $\mathcal{A}$  be value of  $\mathcal{I}_k$  after the update rule if  $(j, k)$  is replaced with  $(i, k)$ . Let  $\mathcal{B}$  be the state of  $\mathcal{I}_k$  after the update rule if we do not allow for swapping.  $\mathcal{A}$  and  $\mathcal{B}$  are then given by

$$\mathcal{A} = \tilde{w}_{ik} Z_i + \sum_{(u,k) \in \mathcal{E}, u \neq i,j} \tilde{w}_{uk} Z_u, \quad \mathcal{B} = \tilde{w}_{jk} Z_j + \sum_{(u,k) \in \mathcal{E}, u \neq i,j} \tilde{w}_{uk} Z_u. \quad (3)$$

Additionally, let  $g = -\alpha \frac{\partial \mathcal{L}}{\partial \mathcal{I}_k}$  be the direction in which the loss most steeply descends with respect to  $\mathcal{I}_k$ . By Lemma 1 (Section D of the Appendix) it suffices to show that moving  $\mathcal{I}_k$  towards  $\mathcal{A}$  is more aligned with  $g$  than moving  $\mathcal{I}_k$  towards  $\mathcal{B}$ . Formally we wish to show that

$$\langle \mathcal{A} - \mathcal{I}_k, g \rangle \geq \langle \mathcal{B} - \mathcal{I}_k, g \rangle \quad (4)$$

which simplifies to

$$\tilde{w}_{ik} \langle Z_i, g \rangle \geq \tilde{w}_{jk} \langle Z_j, g \rangle \quad (5)$$

$$\iff \tilde{w}_{ik}(\tilde{w}_{ik} - w_{ik}) \geq \tilde{w}_{jk}(\tilde{w}_{jk} - w_{jk}). \quad (6)$$

In the case where  $\tilde{w}_{ik}$  and  $(\tilde{w}_{jk}-w_{jk})$  have the same sign but  $\tilde{w}_{jk}$  and  $(\tilde{w}_{jk}-w_{jk})$  have different signs the inequality immediately holds. This corresponds to the case where  $w_{ik}$  *increases* in magnitude but  $w_{jk}$  *decreases* in magnitude. The opposite scenario ( $w_{ik}$  *decreases* in magnitude but  $w_{jk}$  *increases*) is impossible since  $|w_{ik}| < |w_{jk}|$  but  $|\tilde{w}_{ik}| > |\tilde{w}_{jk}|$ .

We now consider the scenario where both sides of the inequality (equation 6) are positive. Simplifying further we obtain

$$(\tilde{w}_{jk}w_{jk} - \tilde{w}_{ik}w_{ik}) \geq (\tilde{w}_{jk}^2 - \tilde{w}_{ik}^2) \quad (7)$$

and are now able to identify a range for  $\alpha$  such that the inequality above is satisfied. By assumption the right hand side is less than 0 and  $\text{sign}(\tilde{w}) = \text{sign}(w)$  so  $\tilde{w}w = |\tilde{w}||w|$ . Accordingly, it suffices to show that

$$|\tilde{w}_{jk}||w_{jk}| - |\tilde{w}_{ik}||w_{ik}| \geq 0. \quad (8)$$

If we let  $\epsilon = |w_{jk}| - |w_{ik}|$  and  $\alpha^* = \sup\{\alpha : |\tilde{w}_{ik}| \leq |\tilde{w}_{jk}| + \epsilon|\tilde{w}_{jk}||\tilde{w}_{ik}|^{-1}\}$ , then for  $\alpha \in (0, \alpha^*)$

$$|\tilde{w}_{jk}||w_{jk}| - |\tilde{w}_{ik}||w_{ik}| \geq |\tilde{w}_{jk}| \left( \underbrace{|w_{jk}| - |w_{ik}|}_{=\epsilon} - \epsilon \right) = 0 \quad (9)$$

the inequality (equation 7) is satisfied. Here we are implicitly using our assumption that the gradient is bounded and we may “tune”  $\alpha$  to control the magnitude  $|\tilde{w}_{ik}| - |\tilde{w}_{jk}|$ . In the case where  $\alpha = \inf\{\alpha : |\tilde{w}_{ik}| > |\tilde{w}_{jk}|\}$  the right hand side of equation 7 becomes 0 while the left hand side is  $\epsilon > 0$ .

### 2.3 Dynamic Neural Graph

We now consider a more general setting where the state of each node  $Z_v(t)$  may vary through time. We refer to this model as a *dynamic neural graph*.

The initial conditions of a *dynamic neural graph* are given by

$$Z_v(0) = \begin{cases} g_\phi^{(v)}(\mathcal{X}) & v \in \mathcal{V}_0 \\ 0 & v \in \mathcal{V} \setminus \mathcal{V}_0 \end{cases} \quad (10)$$

where  $\mathcal{V}_0$  is a designated set of input nodes, which may now have parents.

**Discrete Time Dynamics:** For a discrete time neural graph we consider times  $\ell \in \{0, 1, \dots, L\}$ . The dynamics are then given by

$$Z_v(\ell + 1) = f_{\theta_v} \left( \sum_{(u,v) \in \mathcal{E}} w_{uv} Z_u(\ell), \ell \right) \quad (11)$$

and the network output is  $\hat{\mathcal{Y}} = h_\psi(\mathbf{Z}_{\mathcal{V}_E}(L))$ . We may express equation 11 more succinctly as

$$\mathbf{Z}_{\mathcal{V}}(\ell + 1) = \mathbf{f}_\theta(\mathcal{A}_{\mathcal{G}}\mathbf{Z}_{\mathcal{V}}(\ell), \ell) \quad (12)$$

where  $\mathbf{Z}_{\mathcal{V}}(\ell) = (Z_v(\ell))_{v \in \mathcal{V}}$ ,  $\mathbf{f}_\theta(\mathbf{z}, \ell) = (f_{\theta_v}(z_v, \ell))_{v \in \mathcal{V}}$ , and  $\mathcal{A}_{\mathcal{G}}$  is the weighted adjacency matrix for graph  $\mathcal{G}$ . Equation 12 suggests the following interpretation: At each time step we send information through the edges using  $\mathcal{A}_{\mathcal{G}}$  then apply a function at each node.

**Continuous Time Dynamics:** As in [2], we consider the case where  $t$  may take on a continuous range of values. We then arrive at dynamics given by

$$\nabla \mathbf{Z}_{\mathcal{V}}(t) = \mathbf{f}_\theta(\mathcal{A}_{\mathcal{G}}\mathbf{Z}_{\mathcal{V}}(t), t). \quad (13)$$

Interestingly, if  $\mathcal{V}_0$  is a strict subset of  $\mathcal{V}$  we uncover an Augmented Neural ODE [5].

The discrete time case is unifying in the sense that it may also express any static neural graph. In Figure 1 we illustrate that an MLP may also be expressed by a discrete time neural graph. Additionally, the discrete time dynamics are able to capture sequential models such as LSTMs [9], as long as we allow input to flow into  $\mathcal{V}_0$  at any time.

In continuous time it is not immediately obvious how to incorporate strided convolutions. One approach is to keep the same spatial resolution throughout and pad with zeros after applying strided convolutions. This design is illustrated by Figure 2.

We may also apply Algorithm 1 to learn the structure of dynamic neural graphs. One may use backpropagation through time [26] and the adjoint-sensitivity method [2] for optimization in the discrete and continuous time settings respectively. In Section 3.1, we demonstrate empirically that our method performs better than a random graph, though we do not formally justify the application of our algorithm in this setting.

## 2.4 Implementation details for Large Scale Experiments

For large scale experiments we do not consider the dynamic case as optimization is too expensive. Accordingly, we now present our method for constructing a large and efficient *static neural graph*. With this model we may jointly learn the structure of the graph along with the parameters on ImageNet [4]. As illustrated by Table 4 our model closely follows the structure of MobileNetV1 [10], and so we refer to it as MobileNetV1-DNW. We consider a separate *neural graph* for each spatial resolution – the output of graph  $\mathcal{G}_i$  is the input of graph  $\mathcal{G}_{i+1}$ . For width multiplier [10]  $d$  and spatial resolution  $s \times s$  we constrain MobileNetV1-DNW to have the same number of edges for resolution  $s \times s$  as the corresponding MobileNetV1  $\times d$ . We use a *slightly smaller* width multiplier to obtain a model with similar FLOPs as we do not explicitly reduce the number of depthwise convolutions in MobileNetV1-DNW. However, we do find that neurons often *die* (have no output) and we may then skip the depthwise convolution during inference. Note that if we interpret a pointwise convolution with  $c_1$  input channels and  $c_2$  output channels as a complete bipartite graph then the number of edges is simply  $c_1 * c_2$ .

We also constrain the longest path in graph  $\mathcal{G}$  to be equivalent to the number of layers of the corresponding MobileNetV1. We do so by partitioning the nodes  $\mathcal{V}$  into blocks  $\mathcal{B} = \{\mathcal{B}_0, \dots, \mathcal{B}_{L-1}\}$  where  $\mathcal{B}_0$  is the input nodes  $\mathcal{V}_0$ ,  $\mathcal{B}_{L-1}$  is output nodes  $\mathcal{V}_E$ , and we only allow edges between nodes in  $\mathcal{B}_i$  and  $\mathcal{B}_j$  if  $i < j$ . The longest path in a graph with  $L$  blocks is then  $L - 1$ . Splitting the graph into Blocks also improves efficiency as we may operate on one block at a time. The structure of MobileNetV1 may be recovered by considering a complete bipartite graph between adjacent blocks.

The operation  $f_{\theta_v}$  at each non-output node is a batch-norm [12] (2 parameters), ReLU [14],  $3 \times 3$  convolution (9 parameters) triplet. There are no operations at the output nodes. When the spatial resolution decreases in MobileNetV1 we change the convolutional stride of the input nodes to 2.

In models denoted MobileNetV1-DNW-Small ( $\times d$ ) we also limit the last fully connected (FC) layer to have the same number of edges as the FC layer in MobileNetV1 ( $\times d$ ). In the normal setting of MobileNetV1-DNW we do not modify the last FC layer.

## 3 Experiments

In this section we demonstrate the effectiveness of DNW for image classification in small and large scale settings. We begin by comparing our method with a random wiring on a small scale dataset and model. This allows us to experiment in static, discrete time, and continuous settings. Next we explore the use of DNW at scale with experiments on ImageNet [4]. Finally, we compare DNW with other methods of discovering network structures.

Throughout this section we let RG denote our primary baseline – a **randomly wired graph**. To construct a randomly wired graph with  $k$ -edges we assign a uniform random weight to each edge then pick the  $k$  edges with the largest magnitude weights. As shown in [28], random graphs often outperform manually designed networks.

### 3.1 Small Scale Experiments For Static and Dynamic Neural Graphs

We begin by training tiny classifiers for the CIFAR-10 dataset [13]. Our initial aim is not to achieve state of the art performance but instead to explore DNW in the static, discrete, and continuous time settings. As illustrated by Table 1, our method outperforms a random graph by a large margin.

Table 1: Testing a tiny (41k parameters) classifier on CIFAR-10 [13] in static and dynamic settings shown as mean and standard deviation (std) over 5 runs.

Model	Accuracy
Static (RG)	$76.1 \pm 0.5\%$
Static (DNW)	$80.9 \pm 0.6\%$
Discrete Time (RG)	$77.3 \pm 0.7\%$
Discrete Time (DNW)	$82.3 \pm 0.6\%$
Continuous (RG)	$78.5 \pm 1.2\%$
Continuous (DNW)	$83.1 \pm 0.3\%$

Table 2: Other methods for discovering wirings (using the architecture described in Table 4) tested on CIFAR-10 shown as mean and std over 5 runs. Models with  $\dagger$  first require the complete graph to be trained.

Model	Accuracy
MobileNetV1 ( $\times 0.25$ )	$86.3 \pm 0.2\%$
MobileNetV1-RG( $\times 0.225$ )	$87.2 \pm 0.1\%$
No Update Rule	$86.7 \pm 0.5\%$
L1 + Anneal	$84.3 \pm 0.6\%$
TD $\rho = 0.75$	$87.8 \pm 0.4\%$
TD $\rho = 0.9$	$89.0 \pm 0.2\%$
TD $\rho = 0.95$	$89.2 \pm 0.4\%$
TD $\rho = 0.99$	$88.6 \pm 0.2\%$
TD $\rho = \gamma$	$88.8 \pm 0.2\%$
Lottery Ticket (one-shot) $\dagger$	$87.9 \pm 0.3\%$
Fine Tune $\alpha = 0.1^\dagger$	$89.4 \pm 0.2\%$
Fine Tune $\alpha = 0.01^\dagger$	$89.7 \pm 0.1\%$
Fine Tune $\alpha = 0.001^\dagger$	$88.7 \pm 0.2\%$
MobileNetV1-DNW( $\times 0.225$ )	$89.7 \pm 0.2\%$

The image is first downsampled<sup>3</sup> then each channel is given as input to a node in a *neural graph*. The static graph uses 5 blocks and the discrete time graph uses 5 time steps. For the continuous case we backprop through the operation of an adaptive ODE solver<sup>4</sup>. The models have 41k parameters. At each node we perform Instance Normalization [25], ReLU, and a  $3 \times 3$  single channel convolution.

### 3.2 ImageNet Classification

For large scale experiments on ImageNet [4] we are limited to exploring DNW in the static case (recurrent and continuous time networks are more expensive to optimize due to lack of parallelization). Although our network follows the simple structure of MobileNetV1 [10] we are able to achieve higher accuracy than modern networks which are more advanced and optimized. Notably, MobileNetV2 [22] extends MobileNetV1 by adding residual connections and linear bottlenecks and ShuffleNet [29, 19] introduces channel splits and channel shuffles. The results of the large scale experiments may be found in Table 3.

As standard, we have divided the results of Table 3 to consider models which have similar FLOPs. In the more sparse case ( $\sim 41\text{M}$  FLOPs) we are able to use DNW to boost the performance of MobileNetV1 by 10%. Though random graphs perform extremely well we still observe a 7% boost in performance. In each experiment we train for 250 epochs using Cosine Annealing as the learning rate scheduler with initial learning rate 0.1, as in [28]. Models using random graphs have considerably more FLOPs as nearly all depthwise convolutions must be performed. DNW allows neurons to die and we may therefore skip many operations.

### 3.3 Related Methods

We compare DNW with various methods for discovering neural wirings. In Table 2 we use the structure of MobileNetV1-DNW but try other methods which find  $k$ -edge sub-networks. The experiments in Table 2 are conducted using CIFAR-10 [13]. We train for 160 epochs using Cosine Annealing as the learning rate scheduler with initial learning rate  $\alpha = 0.1$  unless otherwise noted.

**The Lottery Ticket Hypothesis:** The authors of [6, 7] offer an intriguing hypothesis: sparse sub-networks may be trained in isolation. However, their method for finding so-called winning tickets is quite expensive as it requires training the full graph from scratch. We compare with **one-shot** pruning from [7]. One-shot pruning is more comparable in training FLOPs than iterative pruning [6], though both methods are more expensive in training FLOPs than DNW. After training the full network  $\mathcal{G}_{\text{full}}$

<sup>3</sup>We use two  $3 \times 3$  strided convolutions. The first is standard while the second is depthwise-separable.

<sup>4</sup>We use a 5th order Runge-Kutta method [23] as implemented by [2] (from  $t = 0$  to 1 with tolerance 0.001).

Table 3: ImageNet Experiments (see Section 2.4 for more details). Models with \* use the implementations of [19]. Models with multiples asterisks use different image resolutions so that the FLOPs is comparable (see Table 8 in [19] for more details).

Model	Params	FLOPs	Accuracy
MobileNetV1 ( $\times 0.25$ ) [10]	0.5M	41M	50.6%
MobileNetV2 ( $\times 0.15$ )* [22]	—	39M	44.9%
MobileNetV2 ( $\times 0.4$ )**	—	43M	56.6%
DenseNet ( $\times 0.5$ )* [11]	—	42M	41.1%
Xception ( $\times 0.5$ )* [3]	—	40M	55.1%
ShuffleNetV1 ( $\times 0.5$ , $g = 3$ ) [29]	—	38M	56.8%
ShuffleNetV2 ( $\times 0.5$ ) [19]	1.4M	41M	60.3%
MobileNetV1-RG( $\times 0.225$ )	1.2M	55.7M	53.3%
MobileNetV1-DNW-Small ( $\times 0.15$ )	0.24M	22.1M	50.3%
MobileNetV1-DNW-Small ( $\times 0.225$ )	0.4M	41.2M	59.9%
MobileNetV1-DNW( $\times 0.225$ )	1.1M	42.1M	60.9%
MnasNet-search1 [24]	1.9M	65M	64.9%
MobileNetV1-DNW( $\times 0.3$ )	1.3M	66.7M	65.0%
MobileNetV1 ( $\times 0.5$ )	1.3M	149M	63.7%
MobileNetV2 ( $\times 0.6$ )*	—	141M	66.6%
MobileNetV2 ( $\times 0.75$ )***	—	145M	67.9%
DenseNet ( $\times 1$ )*	—	142M	54.8%
Xception ( $\times 1$ )*	—	145M	65.9%
ShuffleNetV1 ( $\times 1$ , $g = 3$ )	—	140M	67.4%
ShuffleNetV2 ( $\times 1$ )	2.3M	146M	69.4%
MobileNetV1-RG( $\times 0.49$ )	1.8M	170M	64.1%
MobileNetV1-DNW( $\times 0.49$ )	1.8M	154M	70.4%

(i.e. no edges pruned) the optimal sub-network  $\mathcal{G}_k$  with  $k$ -edges is chosen by taking the weights with the highest magnitude. In the row denoted *Lottery Ticket* we retrain  $\mathcal{G}_k$  using the initialization of  $\mathcal{G}_{\text{full}}$ . We found it better to initialize  $\mathcal{G}_k$  with the weights of  $\mathcal{G}_{\text{full}}$  after training – denoted by **FT** for *fine-tune* (we try different initial learning rates  $\alpha$ ). Though these experiments perform comparably with DNW, their training is much more expensive as the full graph must initially be trained.

**Exploring Randomly Wired Networks for Image Recognition:** The authors of [28] explore “a more diverse set of connectivity patterns through the lens of randomly wired neural networks.” They achieve impressive performance on ImageNet [4] using random graph algorithms to generate the structure of a neural network. Their network connectivity, however, is fixed during training. Throughout this section we have a random graph (denoted **RG**) as our primary baseline – as in [28] we have seen that random graphs outperform hand-designed networks.

**No Update Rule:** In this ablation on DNW we do not apply the update rule to the hallucinated edges. An edge may only leave the hallucinated edge set if the magnitude of a real edge is sufficiently *decreased*. This experiment demonstrates the importance of the update rule.

**L1 + Anneal:** We experiment with a simple pruning technique – start with a fully connected graph and remove edges by magnitude throughout training until there are only  $k$  remaining. We found that accuracy was much better if we added an L1 regularization term.

**Targeted Dropout:** The authors of [8] present a simple and effective method for training a network which is robust to subsequent pruning. Their method outperforms variational dropout [20] and  $L_0$  pruning [18]. We compare with *Weight Dropout/Pruning* from [8], which we denote as **TD**. Their method is as follows: choose the bottom  $\gamma$  fraction of weights by magnitude<sup>5</sup> and apply dropout with probability  $\rho$ . We use the same architecture as MobileNetV1-DNW ( $\times 0.225$ ) and fix  $\gamma$  at each stage so that the network *post pruning* has the same number of edges per stage as MobileNetV1-DNW ( $\times 0.225$ ). As illustrated by Table 2 we experiment with a couple variants of constant  $\rho$  and also try  $\rho = \gamma$ .

<sup>5</sup>In *Weight Dropout/Pruning* from [8] they choose the bottom  $\gamma$  fraction of incoming weights to each neuron. We instead consider the bottom  $\gamma$  fraction of all weights in the graph. As illustrated by the experiments in Section B of the Appendix, we observe that this performs better in the considered setting.



**Neural Architecture Search:** As illustrated by Table 3, our network (with a very simple MobileNetV1 like structure) is able to achieve comparable accuracy to an expensive method which performs neural architecture search using reinforcement learning [24].

## 4 Scope & Limitations

**Efficiency:** Our training process is still more expensive than training a sparse sub-network in isolation – on the backwards pass we must consider the complete graph. For this reason our large scale experiments are still limited to the small FLOP regimes. In the future we hope to explore more stochastic methods where we only update a “mini-batch” of weight values.

**Locality:** Our algorithm is quite simple and *local*. We anticipate that methods of discovering neural wirings which take global structure into account may perform better. We look forward to exploring these methods in future work.

## 5 Conclusion

We present a novel method for discovering neural wirings. With a simple algorithm we demonstrate a significant boost in accuracy over randomly wired networks. Just as in [28], our networks are free from the typical constraints of NAS. This work suggests exciting directions for more complex and efficient methods of discovering neural wirings.

### Acknowledgments

We thank Sarah Pratt, Mark Yatskar and the Beaker team. Computations on `beaker.org` were supported in part by credits from Google Cloud.

## References

- [1] Han Cai, Ligeng Zhu, and Song Han. ProxylessNAS: Direct neural architecture search on target task and hardware. In *ICLR*, 2019.
- [2] Tian Qi Chen, Yulia Rubanova, Jesse Bettencourt, and David K. Duvenaud. Neural ordinary differential equations. In *NeurIPS*, 2018.
- [3] François Chollet. Xception: Deep learning with depthwise separable convolutions. *2017 IEEE Conference on Computer Vision and Pattern Recognition (CVPR)*, pages 1800–1807, 2017.
- [4] Jia Deng, Wei Dong, Richard Socher, Li-Jia Li, Kai Li, and Li Fei-Fei. Imagenet: A large-scale hierarchical image database. In *CVPR 2009*, 2009.
- [5] Emilien Dupont, Arnaud Doucet, and Yee Whye Teh. Augmented neural odes. *CoRR*, abs/1904.01681, 2019.
- [6] Jonathan Frankle and Michael Carbin. The lottery ticket hypothesis: Finding sparse, trainable neural networks. In *ICLR 2019*, 2019.
- [7] Jonathan Frankle, Gintare Karolina Dziugaite, Daniel M. Roy, and Michael Carbin. The lottery ticket hypothesis at scale. *CoRR*, abs/1903.01611, 2019.
- [8] Aidan N. Gomez, Ivan Zhang, Kevin Swersky, Yarin Gal, and Geoffrey E. Hinton. Learning sparse networks using targeted dropout, 2019.
- [9] Sepp Hochreiter and Jürgen Schmidhuber. Long short-term memory. *Neural Computation*, 9:1735–1780, 1997.
- [10] Andrew G. Howard, Menglong Zhu, Bo Chen, Dmitry Kalenichenko, Weijun Wang, Tobias Weyand, Marco Andreetto, and Hartwig Adam. Mobilenets: Efficient convolutional neural networks for mobile vision applications. *CoRR*, abs/1704.04861, 2017.
- [11] Gao Huang, Zhuang Liu, and Kilian Q. Weinberger. Densely connected convolutional networks. *2017 IEEE Conference on Computer Vision and Pattern Recognition (CVPR)*, pages 2261–2269, 2017.
- [12] Sergey Ioffe and Christian Szegedy. Batch normalization: Accelerating deep network training by reducing internal covariate shift. In *ICML*, 2015.
- [13] Alex Krizhevsky. Learning multiple layers of features from tiny images. Technical report, University of Toronto, 2009.

- [14] Alex Krizhevsky, Ilya Sutskever, and Geoffrey E. Hinton. Imagenet classification with deep convolutional neural networks. *Commun. ACM*, 60:84–90, 2012.
- [15] Anders Krogh and John A. Hertz. A simple weight decay can improve generalization. In *NIPS*, 1991.
- [16] Chenxi Liu, Barret Zoph, Maxim Neumann, Jonathon Shlens, Wei Hua, Li-Jia Li, Li Fei-Fei, Alan Yuille, Jonathan Huang, and Kevin Murphy. Progressive neural architecture search. In *Proceedings of the European Conference on Computer Vision (ECCV)*, pages 19–34, 2018.
- [17] Hanxiao Liu, Karen Simonyan, and Yiming Yang. Darts: Differentiable architecture search. *CoRR*, abs/1806.09055, 2019.
- [18] Christos Louizos, Max Welling, and Diederik P. Kingma. Learning sparse neural networks through  $l_0$  regularization. *CoRR*, abs/1712.01312, 2018.
- [19] Ningning Ma, Xiangyu Zhang, Hai-Tao Zheng, and Jian Sun. Shufflenet v2: Practical guidelines for efficient cnn architecture design. In *ECCV*, 2018.
- [20] Dmitry Molchanov, Arsenii Ashukha, and Dmitry P. Vetrov. Variational dropout sparsifies deep neural networks. In *ICML*, 2017.
- [21] David E. Rumelhart, Geoffrey E. Hinton, and Ronald J. Williams. Learning representations by back-propagating errors. *Nature*, 323:533–536, 1986.
- [22] Mark B. Sandler, Andrew G. Howard, Menglong Zhu, Andrey Zhmoginov, and Liang-Chieh Chen. Mobilenetv2: Inverted residuals and linear bottlenecks. *2018 IEEE/CVF Conference on Computer Vision and Pattern Recognition*, pages 4510–4520, 2018.
- [23] F Shampine, Lawrence. Some practical runge-kutta formulas. *Math. Comput.*, 46(173):135–150, January 1986.
- [24] Mingxing Tan, Bo Chen, Ruoming Pang, Vijay Vasudevan, and Quoc V. Le. Mnasnet: Platform-aware neural architecture search for mobile. *CoRR*, abs/1807.11626, 2018.
- [25] Dmitry Ulyanov, Andrea Vedaldi, and Victor S. Lempitsky. Instance normalization: The missing ingredient for fast stylization. *CoRR*, abs/1607.08022, 2016.
- [26] P. J. Werbos. Backpropagation through time: what it does and how to do it. *Proceedings of the IEEE*, 78(10):1550–1560, Oct 1990.
- [27] Bichen Wu, Xiaoliang Dai, Peizhao Zhang, Yanghan Wang, Fei Sun, Yiming Wu, Yuandong Tian, Peter Vajda, Yangqing Jia, and Kurt Keutzer. Fbnet: Hardware-aware efficient convnet design via differentiable neural architecture search. *arXiv preprint arXiv:1812.03443*, 2018.
- [28] Saining Xie, Alexander Kirillov, Ross B. Girshick, and Kaiming He. Exploring randomly wired neural networks for image recognition. *CoRR*, abs/1904.01569, 2019.
- [29] Xiangyu Zhang, Xinyu Zhou, Mengxiao Lin, and Jian Sun. Shufflenet: An extremely efficient convolutional neural network for mobile devices. *2018 IEEE/CVF Conference on Computer Vision and Pattern Recognition*, pages 6848–6856, 2018.
- [30] Barret Zoph and Quoc V Le. Neural architecture search with reinforcement learning. *arXiv preprint arXiv:1611.01578*, 2016.

## A Architecture

Table 4: The general structure of MobileNetV1 vs. MobileNetV1-DNW for ImageNet experiments. *dwconv* denotes *depthwise convolutions*, *pwconv* denotes *pointwise convolution*, FC denotes a fully connected layer,  $d$  denotes width multiplier [10],  $c$  denotes the number of output channels, and  $s$  denotes stride. When omitted assume that stride is 1. Batch-norm [12] and ReLU follow each convolution in MobileNetV1. When training on CIFAR-10 [13] the first convolution has stride 1.

Stage	Output	MobilNetV1	MobileNetV1-DNW
0	$112 \times 112$	$3 \times 3$ conv, $c = 32d$ , $s = 2$	$g_\phi = (3 \times 3$ conv, $c = 32$ , $s = 2)$
1	$112 \times 112$	$3 \times 3$ <i>dwconv</i> , $c = 32d$ $3 \times 3$ <i>pwconv</i> , $c = 64d$	$\mathcal{G}_1$ with $ \mathcal{V}  = 32 + 64$ $ \mathcal{V}_0  = 32$ , $ \mathcal{V}_E  = 64$ , $ \mathcal{B}  = 2$
2	$56 \times 56$	$3 \times 3$ <i>dwconv</i> , $c = 64d$ , $s = 2$ $3 \times 3$ <i>pwconv</i> , $c = 128d$ $3 \times 3$ <i>dwconv</i> , $c = 128d$ $3 \times 3$ <i>pwconv</i> , $c = 128d$	$\mathcal{G}_2$ with $ \mathcal{V}  = 64 + 2 * 128$ $ \mathcal{V}_0  = 64$ , $ \mathcal{V}_E  = 128$ , $ \mathcal{B}  = 3$
3	$28 \times 28$	$3 \times 3$ <i>dwconv</i> , $c = 128d$ , $s = 2$ $3 \times 3$ <i>pwconv</i> , $c = 256d$ $3 \times 3$ <i>dwconv</i> , $c = 256d$ $3 \times 3$ <i>pwconv</i> , $c = 256d$	$\mathcal{G}_3$ with $ \mathcal{V}  = 128 + 2 * 256$ $ \mathcal{V}_0  = 128$ , $ \mathcal{V}_E  = 256$ , $ \mathcal{B}  = 3$
4	$14 \times 14$	$3 \times 3$ <i>dwconv</i> , $c = 256d$ , $s = 2$ $3 \times 3$ <i>pwconv</i> , $c = 512d$  $5 \times \begin{cases} 3 \times 3$ <i>dwconv</i> , $c = 512d$ \\ $3 \times 3$ <i>pwconv</i> , $c = 512d$ \end{cases}	$\mathcal{G}_4$ with $ \mathcal{V}  = 256 + 6 * 512$ $ \mathcal{V}_0  = 256$ , $ \mathcal{V}_E  = 512$ , $ \mathcal{B}  = 7$
5	$7 \times 7$	$3 \times 3$ <i>dwconv</i> , $c = 512d$ , $s = 2$ $3 \times 3$ <i>pwconv</i> , $c = 1024d$ $3 \times 3$ <i>dwconv</i> , $c = 1024d$ $3 \times 3$ <i>pwconv</i> , $c = 1024d$	$\mathcal{G}_5$ with $ \mathcal{V}  = 512 + 2 * 1024$ $ \mathcal{V}_0  = 512$ , $ \mathcal{V}_E  = 1024$ , $ \mathcal{B}  = 3$
6	1000	$7 \times 7$ pool, $1024d \times 1000$ FC	$h_\psi = (7 \times 7$ pool, $1024 \times 1000$ FC)

## B Targeted Dropout: Regular and Unconstrained

In the setting we consider, unconstrained targeted *weight dropout* outperforms the targeted *weight dropout* presented in [8] (which we refer to as *regular*). Accordingly, the results we present in Table 2 correspond to unconstrained targeted *weight dropout*. In regular targeted *weight dropout*, dropout is applied to the bottom  $\gamma$  fraction of incoming weights *to each neuron*. In unconstrained targeted *weight dropout*, we apply dropout to the bottom  $\gamma$  fraction of edges at the spatial resolution. Accordingly, neurons may die and have no incoming or outgoing edges. We compare unconstrained and regular targeted dropout in Table 5.

Table 5: Comparing variants of targeted weight dropout using the architecture described in Table 4 and tested on CIFAR-10 shown as mean and std over 5 runs.

Model	Accuracy (Unconstrained)	Accuracy (Regular)
TD $\rho = 0.9$	$89.0 \pm 0.2\%$	$87.9 \pm 0.5\%$
TD $\rho = 0.95$	$89.2 \pm 0.4\%$	$87.9 \pm 0.2\%$
TD $\rho = 0.99$	$88.6 \pm 0.2\%$	$87.7 \pm 0.3\%$
TD $\rho = \gamma$	$88.8 \pm 0.2\%$	$87.9 \pm 0.2\%$

## C A More General Case

We now consider the case where the *hallucinated edge*  $(i, \ell)$  replaces  $(j, k) \in \mathcal{E}$ .

As before we use  $\tilde{w}$  to denote the weight  $w$  after the weight update rule  $\tilde{w}_{uv} = w_{uv} + \left\langle Z_u, -\alpha \frac{\partial \mathcal{L}}{\partial \mathcal{I}_v} \right\rangle$ . We assume that  $\alpha$  is small enough so that  $\text{sign}(\tilde{w}) = \text{sign}(w)$ .

**Claim:** Assume  $\mathcal{L}$  is Lipschitz continuous. There exists a learning rate  $\alpha^* > 0$  such that for  $\alpha \in (0, \alpha^*)$  the process of swapping  $(i, \ell)$  for  $(j, k)$  will decrease the loss when the state of the nodes are fixed, there is no path from  $i$  to  $j$ , and  $|w_{i\ell}| < |w_{jk}|$  but  $|\tilde{w}_{i\ell}| > |\tilde{w}_{jk}|$ .

*Proof.* Let  $\mathcal{A}_k, \mathcal{A}_\ell$  be value of  $\mathcal{I}_k$  and  $\mathcal{I}_\ell$  after the update rule if  $(j, k)$  is replaced with  $(i, \ell)$ . Let  $\mathcal{B}_k$  and  $\mathcal{B}_\ell$  be the state of  $\mathcal{I}_k$  and  $\mathcal{I}_\ell$  after the update rule if we do not allow for swapping.  $\mathcal{A}_k, \mathcal{A}_\ell, \mathcal{B}_k$  and  $\mathcal{B}_\ell$  are then given by

$$\mathcal{A}_k = \sum_{(u,k) \in \mathcal{E}, u \neq j} \tilde{w}_{uk} Z_u, \quad \mathcal{B}_k = \tilde{w}_{jk} Z_j + \sum_{(u,k) \in \mathcal{E}, u \neq j} \tilde{w}_{uk} Z_u \quad (14)$$

$$\mathcal{A}_\ell = \tilde{w}_{i\ell} Z_i + \sum_{(u,\ell) \in \mathcal{E}, u \neq i} \tilde{w}_{u\ell} Z_u, \quad \mathcal{B}_\ell = \sum_{(u,\ell) \in \mathcal{E}, u \neq i} \tilde{w}_{u\ell} Z_u. \quad (15)$$

Additionally, let  $g_k = -\alpha \frac{\partial \mathcal{L}}{\partial \mathcal{I}_k}$  and  $g_\ell = -\alpha \frac{\partial \mathcal{L}}{\partial \mathcal{I}_\ell}$  be the direction in which the loss most steeply descends with respect to  $\mathcal{I}_k$  and  $\mathcal{I}_\ell$ . By *Lemma 1* (Section D of the Appendix) it suffices to show that

$$\langle \mathcal{A}_k - \mathcal{I}_k, g_k \rangle + \langle \mathcal{A}_\ell - \mathcal{I}_\ell, g_\ell \rangle \geq \langle \mathcal{B}_k - \mathcal{I}_k, g_k \rangle + \langle \mathcal{B}_\ell - \mathcal{I}_\ell, g_\ell \rangle \quad (16)$$

which simplifies to

$$\begin{aligned} \tilde{w}_{i\ell} \langle Z_i, g_\ell \rangle &\geq \tilde{w}_{jk} \langle Z_j, g_k \rangle \\ \iff \tilde{w}_{i\ell} (\tilde{w}_{i\ell} - w_{i\ell}) &\geq \tilde{w}_{jk} (\tilde{w}_{jk} - w_{jk}). \end{aligned} \quad (17)$$

We are now in the equivalent setting as equation 6 and may complete the proof as before.

In practice there may be a path from  $i$  and  $j$  the state of the nodes will never be the fixed due to stochasticity of mini-batches and updates to the rest of the parameters in the network. However, as the graph grows large the state of one node will have little effect on the state of another, even if there is a path between them. The proofs are done in an idealized case and the empirical results demonstrate that the method works in practice.

## D Lemma 1

Here we show that for sufficiently small  $\alpha$

$$\left\langle \gamma_1, -\alpha \frac{\partial \mathcal{L}}{\partial Z_v} \right\rangle > \left\langle \gamma_2, -\alpha \frac{\partial \mathcal{L}}{\partial Z_v} \right\rangle \quad (19)$$

implies that

$$\mathcal{L}(\mathcal{I}_v + \alpha \gamma_1) < \mathcal{L}(\mathcal{I}_v + \alpha \gamma_2). \quad (20)$$

Note that for brevity we have written the loss as a function of  $\mathcal{I}_v$ . By taking a Taylor expansion we find that

$$\mathcal{L}(\mathcal{I}_v + \alpha \gamma) \quad (21)$$

$$= \mathcal{L}(\mathcal{I}_v) + \left\langle \alpha \gamma, \frac{\partial \mathcal{L}}{\partial Z_v} \right\rangle + \mathcal{O}(\alpha^2) \quad (22)$$

$$(23)$$

and so for sufficiently small  $\alpha$

$$\mathcal{L}(\mathcal{I}_v) - \mathcal{L}(\mathcal{I}_v + \alpha \gamma) \approx \left\langle \gamma, -\alpha \frac{\partial \mathcal{L}}{\partial Z_v} \right\rangle \quad (24)$$

which completes the lemma.

An equivalent argument holds for two dimensions.

$$\left\langle \gamma_1, -\alpha \frac{\partial \mathcal{L}}{\partial Z_v} \right\rangle + \left\langle \xi_1, -\alpha \frac{\partial \mathcal{L}}{\partial Z_u} \right\rangle > \left\langle \gamma_2, -\alpha \frac{\partial \mathcal{L}}{\partial Z_v} \right\rangle + \left\langle \xi_2, -\alpha \frac{\partial \mathcal{L}}{\partial Z_u} \right\rangle \quad (25)$$

implies that

$$\mathcal{L}(\mathcal{I}_v + \alpha\gamma_1, \mathcal{I}_u + \alpha\xi_1) < \mathcal{L}(\mathcal{I}_v + \alpha\gamma_2, \mathcal{I}_u + \alpha\xi_2). \quad (26)$$

By taking a Taylor expansion we find that

$$\mathcal{L}(\mathcal{I}_v + \alpha\gamma, \mathcal{I}_u + \alpha\xi) \quad (27)$$

$$= \mathcal{L}(\mathcal{I}_v, \mathcal{I}_u) + \left\langle \alpha\gamma, \frac{\partial \mathcal{L}}{\partial Z_v} \right\rangle + \left\langle \alpha\xi, \frac{\partial \mathcal{L}}{\partial Z_u} \right\rangle + \mathcal{O}(\alpha^2) \quad (28)$$

$$(29)$$

and so for sufficiently small  $\alpha$

$$\mathcal{L}(\mathcal{I}_v, \mathcal{I}_u) - \mathcal{L}(\mathcal{I}_v + \alpha\gamma, \mathcal{I}_u + \alpha\xi) \approx \left\langle \gamma, -\alpha \frac{\partial \mathcal{L}}{\partial Z_v} \right\rangle + \left\langle \xi, -\alpha \frac{\partial \mathcal{L}}{\partial Z_u} \right\rangle. \quad (30)$$